

Far-Infrared detection of methylene \star

E. T. Polehampton¹, K. M. Menten¹, S. Brünken², G. Winnewisser², and J.-P. Baluteau³

¹ Max-Planck-Institut für Radioastronomie, Auf dem Hügel 69, D-53121 Bonn, Germany

² Physikalisches Institut, Universität zu Köln, D-50937 Cologne, Germany

³ Laboratoire d’Astrophysique de Marseille, CNRS & Université de Provence, BP 8, F-13376 Marseille Cedex 12, France

Received / accepted

Abstract. We present a clear detection of CH_2 in absorption towards the molecular cloud complexes Sagittarius B2 and W49 N using the ISO Long Wavelength Spectrometer. These observations represent the first detection of its low excitation rotational lines in the interstellar medium. Towards Sagittarius B2, we detect both ortho and para transitions allowing a determination of the total CH_2 column density of $N(\text{CH}_2) = (7.5 \pm 1.1) \times 10^{14} \text{ cm}^{-2}$. We compare this with the related molecule, CH , to determine $[\text{CH}/\text{CH}_2] = 2.7 \pm 0.5$. Comparison with chemical models shows that the CH abundance along the line of sight is consistent with diffuse cloud conditions and that the high $[\text{CH}/\text{CH}_2]$ ratio can be explained by including the effect of grain-surface reactions.

Key words. Infrared: ISM – ISM: molecules – Molecular data – ISM: individual objects: Sagittarius B2 – ISM: individual objects: W49

1. Introduction

Methylene (CH_2) is thought to be a relatively abundant molecule in diffuse as well as in dense interstellar clouds, with similar abundances to CH (e.g. van Dishoeck & Black 1986; Lee et al. 1996). However, it has proved very difficult to detect observationally, mainly due to the inaccessibility of its rotational lines from the ground.

Methylene was initially proposed to explain an unidentified ultraviolet (UV) band observed in comets (Herzberg 1942a,b) but later this band was shown to be associated with C_3 (Douglas 1951). CH_2 remains undetected in comets, but recently, several of its electronic bands have been observed in the interstellar medium (ISM) by Lyu et al. (2001) using the Hubble Space Telescope. They tentatively detected CH_2 absorption bands in the UV spectrum towards two stars, HD154368 and ζ Oph.

Interstellar searches for rotational emission/absorption are hampered by the peculiar spectrum of CH_2 , caused by its lightness and b -type selection rules (Michael et al. 2003). This results in lines at widely varying wavelengths, all of which are either completely unobservable from the ground or are in difficult spectral regions that are at the edges of atmospheric windows or for which there are few telescopes with suitable instrumentation to observe them.

Send offprint requests to: E. Polehampton: e-mail: epoleham@mpifr-bonn.mpg.de

\star Based on observations with ISO, an ESA project with instruments funded by ESA Member States (especially the PI countries: France, Germany, the Netherlands and the United Kingdom) with the participation of ISAS and NASA.

Hollis et al. (1995) have, so far, made the only unambiguous identification of CH_2 in the ISM, confirming their earlier detection (Hollis et al. 1989). They clearly identified the $4_{04} - 3_{13}$ rotational transition with simultaneous measurements of multiple fine-structure features between 68 and 71 GHz. These were detected in emission towards Orion KL and W51 M, both dense “hot core” sources, which provide excitation to the 4_{04} level which is ≈ 215 K above the ground state. The lines occur in a rarely observed spectral region, close to the telluric 55–65 GHz O_2 bands. Accurate frequencies for this transition were measured by Lovas et al. (1983).

Low-excitation rotational transitions occur in the far-infrared (FIR) region, accessible by the Infrared Space Observatory (ISO) satellite (and in the future by SOFIA and Herschel), and around $320 \mu\text{m}$ (940 GHz), a spectral region just being opened from the ground. Although limited laboratory data on the rotational spectrum of CH_2 have existed for many years (Lovas et al. 1983; Sears et al. 1984), much more accurate frequencies are currently being measured at the Cologne Laboratory for Molecular Spectroscopy (Michael et al. 2003; Brünken et al. 2004)

We have used these new data to search for low-lying rotational transitions of CH_2 observed by the ISO Long Wavelength Spectrometer (LWS; Clegg et al. 1996). We clearly detect the strongest fine structure components of transitions from the lowest energy level of both ortho and para CH_2 towards Sagittarius B2 (Sgr B2) and of ortho CH_2 towards W49 N. Both Sgr B2 and W49 are giant molecular cloud complexes emitting strong FIR continuum spectra. This makes them particularly

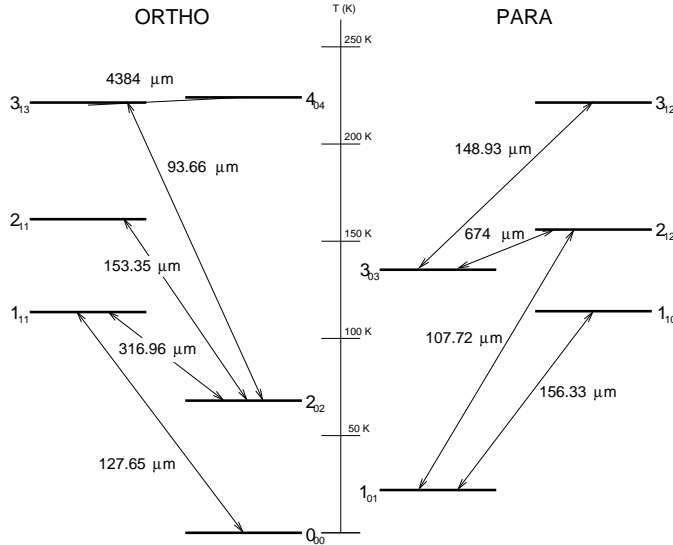


Fig. 1. Low-lying rotational levels of the CH_2 molecule showing the wavelength of the strongest fine structure component for each transition.

good targets for detecting absorption lines from intervening interstellar matter.

Sgr B2 was observed as part of a wide spectral survey using the LWS Fabry-Pérot (FP) mode, allowing us to search for transitions from all the other low-lying energy levels, as well as to compare the data with absorption from the chemically related CH molecule. We use the strong CH lines as a template to fit and calculate column densities for CH_2 . In Sects. 4, 5 and 6 we present the results towards Sgr B2 and in Sect. 7 detail the results for W49 N and several other sources where CH_2 was not detected. We then compare the results with chemical models in Sect. 8.

2. CH_2 rotational spectrum

Figure 1 shows the low-lying rotational states of CH_2 . The energy levels are denoted by N_{KaKc} , where N is the rigid-body rotational quantum number. Each of these levels is split by electron spin-spin and spin-rotation interactions into three fine-structure levels, with the quantum number for total angular momentum excluding nuclear spin, J , equal to $N + 1, N, N - 1$ for $N > 0$ ($J=1$ at $N=0$). Due to the presence of two protons with opposite nuclear spin, CH_2 has both ortho (nuclear spin quantum number, $I=1$) and para ($I=0$) forms. In the ortho levels, the non-zero nuclear spin interacts with the electrons to cause a further hyperfine splitting with total angular momentum quantum number, $F=J + 1, J, J - 1$. Selection rules for rotational transitions are $\Delta J=0, \pm 1$ and $\Delta F=0, \pm 1$.

Frequencies for low-lying rotational transitions have been calculated from Laser Magnetic Resonance (LMR) laboratory spectra by Sears et al. (1984) with a quoted accuracy of 5 MHz (0.6 km s^{-1}). In order to confirm the lines and to calculate accurate line strengths we have used new measurements of the sub-mm lines (Michael et al. 2003; Brünken et al. 2004) to determine more accurate frequency values. Table 1 shows the calculated wavelengths, Einstein coefficients and line strengths

Table 1. Calculated wavelengths, Einstein coefficients (A_{ij}) and line strengths (S_{ij}) for the low-lying transitions of CH_2 (ignoring hyperfine-structure in the ortho transitions). The estimated error corresponding to the last significant figure of the calculated wavelengths is given in parenthesis. The Einstein coefficients and line strengths calculated here are half those given by Sears et al. (1984). The detected lines towards Sgr B2 are shown in bold.

Transition	Wavelength (μm)	A_{ij} (s^{-1})	S_{ij}
$1_{11}-0_{00} J=0-1$	127.31450 (6)	0.0163	0.989
$1_{11}-0_{00} J=1-1$	127.85823 (4)	0.0163	3.02
$1_{11}-0_{00} J=2-1$	127.64614 (5)	0.0163	4.99
$2_{11}-2_{02} J=1-1$	153.102312 (6)	0.0105	3.31
$2_{11}-2_{02} J=1-2$	154.302721 (7)	0.00351	1.14
$2_{11}-2_{02} J=2-1$	152.621311 (6)	0.00217	1.14
$2_{11}-2_{02} J=2-2$	153.814187 (6)	0.00962	5.15
$2_{11}-2_{02} J=2-3$	152.992296 (6)	0.00216	1.14
$2_{11}-2_{02} J=3-2$	154.178941 (6)	0.00151	1.14
$2_{11}-2_{02} J=3-3$	153.352914 (7)	0.0125	9.25
$3_{13}-2_{02} J=2-1$	93.5838 (1)	0.0298	3.60
$3_{13}-2_{02} J=2-2$	94.0309 (1)	0.00559	0.685
$3_{13}-2_{02} J=2-3$	93.7231 (2)	0.000170	0.0205
$3_{13}-2_{02} J=3-2$	93.7025 (2)	0.0317	5.37
$3_{13}-2_{02} J=3-3$	93.3967 (2)	0.00392	0.657
$3_{13}-2_{02} J=4-3$	93.6621 (2)	0.0356	7.75
$1_{10}-1_{01} J=0-1$	156.43947 (1)	0.0133	0.500
$1_{10}-1_{01} J=1-0$	155.66632 (1)	0.00462	0.513
$1_{10}-1_{01} J=1-1$	157.56539 (1)	0.00318	0.366
$1_{10}-1_{01} J=1-2$	156.76825 (1)	0.00548	0.622
$1_{10}-1_{01} J=2-1$	157.12503 (2)	0.00323	0.615
$1_{10}-1_{01} J=2-2$	156.33233 (1)	0.0101	1.88
$2_{12}-1_{01} J=1-0$	107.2947 (2)	0.0134	0.487
$2_{12}-1_{01} J=1-1$	108.1935 (2)	0.0103	0.385
$2_{12}-1_{01} J=1-2$	107.8170 (2)	0.000731	0.0270
$2_{12}-1_{01} J=2-1$	107.8573 (2)	0.0184	1.13
$2_{12}-1_{01} J=2-2$	107.4832 (2)	0.00603	0.367
$2_{12}-1_{01} J=3-2$	107.7203 (2)	0.0244	2.10

(averaging over the hyperfine structure in ortho transitions). The accuracy of the calculated wavelengths is highest for those transitions actually measured in the lab ($2_{11}-2_{02}$ ($153 \mu\text{m}$) and $1_{10}-1_{01}$ ($156 \mu\text{m}$); Brünken et al. 2004). The uncertainty in the calculated Einstein values and line strengths is dominated by that of the dipole moment. We have followed previous authors and used a value of 0.57 D (derived from an ab initio calculation by Bunker & Langhoff 1983). The calculation strongly depends on the electronic and geometric structure of the molecule and inserting the most recent values for the geometry suggests that the uncertainty must be at least 0.02 D (leading to $\sim 5\%$ uncertainty in the Einstein coefficients). The line strength in Table 1 is defined in the same way as by Sears et al. (1984), allowing a direct comparison. This shows that the strengths calculated here are half those previously published. However, our results can reproduce the values for the $1_{11}-2_{02}$ ($317 \mu\text{m}$) transition given by Michael et al. (2003) and agree with the calculations of Chandra (1984) (both of these authors used an independent method to calculate their line strengths). This indicates

Table 2. Coordinates of observed sources.

Source	RA (J2000)	Dec. (J2000)
Sgr B2	17 ^h 47 ^m 21.75 ^s	-28°23'14.1"
W49 N	19 ^h 10 ^m 13.55 ^s	+09°06'14.7"
Sgr A*	17 ^h 45 ^m 39.97 ^s	-29°00'23.6"
NGC7023	21 ^h 01 ^m 36.91 ^s	+68°09'48.2"

that the line strengths quoted in the paper by Sears et al. (1984) are likely to be in error by a factor of two (T. Sears, private communication).

3. Observations and data reduction

The Sgr B2 observations were carried out as part of a wide spectral survey using the ISO LWS Fabry-Pérot (FP) mode, L03. The whole LWS spectral range, from 47 to 196 μm (6.38–1.53 THz), was covered using 36 separate observations with a spectral resolution of 30–40 km s^{-1} . The first results from this survey have recently been presented by Ceccarelli et al. (2002); Polehampton et al. (2002); Vastel et al. (2002); Polehampton et al. (2003). We also analysed additional L04/L03 mode observations towards Sgr B2, W49 N, Sgr A* and NGC7023 and one grating L01 observation towards W49 N, downloaded from the ISO Data Archive¹. Details of the ISO TDT numbers of all the observations used in this paper are shown in Table A.1.

The LWS beam has an effective diameter of $\sim 80''$ (Gry et al. 2003) and was centred on the coordinates shown in Table 2. The coordinates chosen for Sgr B2 were slightly offset from the main FIR peak at Sgr B2 (M) to ensure that Sgr B2 (N) was excluded from the beam. Three positions were observed towards NGC7023 - the illuminating star (coordinates given in Table 2), the NW PDR ($-24.5'', +39.2''$) and the SW PDR ($-25.8'', -63.1''$).

The L03 observations towards Sgr B2 were reduced using the ISO Offline pipeline (OLP) version 8 with the remaining observations processed with OLP version 10 (for FP observations there is no significant difference between OLP 8 and 10). Further processing was then applied interactively using routines that appeared as part of the LWS Interactive Analysis package version 10 (LIA10: Lim et al. 2002) and the ISO Spectral Analysis Package (ISAP: Sturm et al. 1998). The interactive processing included the calculation of accurate dark currents (including stray light), careful removal of the LWS grating profile from the spectra and removal of glitches caused by cosmic ray impacts (see Polehampton et al. 2002, 2003). The wavelength scale of each observation was then corrected to the local standard of rest and data co-added for each line (small multiplicative factors were sometimes necessary to match each observation in flux before co-adding). The final uncertainty in wavelength is less than 0.004 μm (or 11 km s^{-1}) corresponding to the error in absolute wavelength calibration (see Gry et al. 2003). Finally, a polynomial baseline was divided into the data to obtain the line-to-continuum ratio. For the Sgr B2

data, a 3rd order polynomial was necessary to fit the continuum around and between the detected lines. For the L04 data towards W49 N where the continuum coverage is much lower, a 1st order baseline was used. The use of low order polynomials and careful masking of the detected lines for the fit ensured that no spurious features were introduced into the data by the division. This step in the reduction is very useful because it effectively bypasses the large uncertainty in absolute flux level caused by multiplicative calibration steps (see Swinyard et al. 1998). The remaining error is dominated by statistical noise in the data with a small additional uncertainty due to the dark current determination and continuum fit.

In Sect. 6, we use one grating L01 observation towards W49 N to determine the column density of CH. This observation was reduced using OLP 10, and corrected for saturation in the LWS detectors (necessary due to the strength of the W49 N thermal continuum) by T. Grundy at the UK ISO Data Centre. The dataset was further reduced using the LWS L01 post-processing pipeline which performs several additional corrections detailed in Lloyd et al. (2003). This allowed us to calculate an accurate value for the line-to-continuum ratio in the line.

4. Sgr B2 results

We searched the Sgr B2 spectrum for all the low-lying rotational lines of both ortho- and para-CH₂ occurring within the survey range (47–196 μm). Figure 2 shows the data around the three lowest energy transitions (fits to the line shapes are also shown - these are described in Section 4.4). At the spectral resolution of the LWS FP, the fine structure splitting of each rotational transition is resolved but the spacing of the hyperfine components in ortho-CH₂ ($< 10 \text{ km s}^{-1}$) is too small to be separated. When analysing ortho transitions we have used wavelengths averaged over the hyperfine structure weighted by A_{ij} . The wavelengths used are shown in Table 1.

The survey also shows strong absorption due to CH (shown in the top panel of Fig. 2). We have used these lines as a basis for fitting the observed CH₂ line shapes to fix the relative contribution from features along the line of sight. This was necessary because the signal-to-noise in the CH₂ detections is not high enough to allow a full fit accounting for different line of sight components separately. The method assumes that there is a constant [CH/CH₂] ratio applicable to all line of sight components.

4.1. CH

Two prominent absorption features due to CH are present in the spectrum due to its $^2\Pi_{1/2} J=3/2-1/2$ transition from the ground state to the first rotational level, $\sim 96 \text{ K}$ above ground (see also Cernicharo et al. 1999; Goicoechea et al. 2004). These are due to the Λ -doublet type splitting of each rotational level and occur at wavelengths of 149.09 μm and 149.39 μm (Davidson et al. 2001). The two detected lines are shown in the top panel of Fig. 2 and are broad with absorption in the range -150 to $+100 \text{ km s}^{-1}$. This is due to galactic spiral arm clouds between the Sun and Galactic Centre (centred at velocities -100

¹ see <http://www.iso.vilspa.esa.es/ida>.

to $+30 \text{ km s}^{-1}$, e.g. see Greaves & Williams 1994) as well as to Sgr B2 itself. The peak absorption occurs near the velocity of Sgr B2 at $\sim +65 \text{ km s}^{-1}$. These lines have previously been detected with the Kuiper Airborne Observatory (KAO) by Stacey et al. (1987) but the ISO data provide a significant improvement in the signal-to-noise ratio as well as complete coverage of the neighbouring continuum. No higher transitions of CH were detected in the survey above the noise.

In order to determine the CH column density for each velocity component in the line of sight towards Sgr B2, a high resolution model of the line shape was constructed, convolved to the LWS resolution and adjusted to obtain a best fit. This was carried out in the same way as used for OH lines (see Polehampton et al. 2003, Polehampton et al. in preparation). $\text{H}\alpha$ 21 cm absorption measurements (Garwood & Dickey 1989) were used to fix the velocity and line width of 10 line of sight components and then optical depths were adjusted in a multi-parameter fit to find the minimum in χ^2 . The optical depth for each component, τ , was calculated from the line-to-continuum ratio using

$$I = I_c \exp(-\tau) \quad (1)$$

where I_c is the intensity of the continuum. This method assumes that the same velocity components seen in the $\text{H}\alpha$ spectrum are present in CH and CH_2 (but the fit does not depend on the $\text{H}\alpha$ optical depths derived by Garwood & Dickey 1989). This is likely because the atomic material is seen to be associated with molecular gas at the same velocities (e.g. Vastel et al. 2002). Each fitted component probably still represents a mean over many narrower features such as those seen in CS absorption with velocity widths $\sim 1 \text{ km s}^{-1}$ (Greaves & Williams 1994). The final fit is shown in the top panel of Fig. 2.

Column densities for each velocity component are shown in Table 3. These were calculated assuming a Doppler line profile with Maxwellian velocity distribution (e.g. Spitzer 1978),

$$N_j = \frac{8\pi\sqrt{\pi}}{2\sqrt{\ln 2}} 10^{17} \frac{\tau_0 \Delta v}{A_{ij} \lambda_{ij}^3 g_i/g_j} \quad (2)$$

where N_j is the column density in the lower level, τ_0 is the optical depth at line centre, Δv is the line width in km s^{-1} , A_{ij} is the Einstein coefficient for spontaneous emission, λ_{ij} is the wavelength in μm and g_i is the statistical weight of state i .

No higher transitions of CH have been observed in the spectrum even at the velocity of Sgr B2 itself, showing that the level populations are characterised by a low rotation temperature (i.e. sub-thermal excitation) and the ground state population is a good measure of the total column density. Using a 2σ detection limit for the ${}^2\Pi_{1/2} J=5/2-3/2$ CH transition ($116 \mu\text{m}$), we calculate $T_{\text{rot}} < 20 \text{ K}$. The fitted optical depths show that the absorption is generally optically thin, although in the Sgr B2 component at 67 km s^{-1} it is marginally optically thick ($\tau=2.4$). The results of the fit are shown in Fig. 2 and Table 3, with errors determined by examining χ^2 as pairs of optical depths were varied about their best fit values.

One way to check the opacity of Sgr B2 is to use the less abundant ${}^{13}\text{CH}$ isotopomer whose ${}^2\Pi_{1/2} J=3/2-1/2$ transition has components at $149.79 \mu\text{m}$ and $150.09 \mu\text{m}$ (Davidson et al.

Table 3. Results of our fit of the CH lines towards Sgr B2 are given in column (A). The velocities and line widths are taken from the $\text{H}\alpha$ data of Garwood & Dickey (1989). Column (B) gives the previous estimates of CH column densities from the KAO measurements of Stacey et al. (1987) and columns (C) and (D) give the results from the radio Λ -doublet lines from Genzel et al. (1979) and Andrew et al. (1978).

LSR Velocity (km s^{-1})	FWHM (km s^{-1})	$N(\text{CH}) (10^{14} \text{ cm}^{-2})$			
		(A)	(B)	(C)	(D)
-107.6	7	0.9 \pm 0.7	4.2		
-81.7	28	2.6 \pm 1.1			2.5
-51.9	17	0.3 \pm 0.15			
-44.0	8	1.5 \pm 0.6	3.6		1.3
-24.4	14	1.9 \pm 0.4			0.3
+1.1 ^a	19	2.0 \pm 0.3	3.2		1.1
+15.7	7	3.1 \pm 0.8			1.5
+31.4	21	1.5 \pm 1.0			
+52.8/ + 66.7 ^b	11/16	9.3 \pm 0.9	5.2	3.1	9.4 ^c
Total			20.1	15.2	16.1

^a This velocity is corrected from an error in Garwood & Dickey (1989) where it is given as $+11 \text{ km s}^{-1}$

^b The $\text{H}\alpha$ data resolve 2 components in Sgr B2. However, our fit requires only one of these (at 66.7 km s^{-1}) to reproduce the ISO spectrum.

^c This is the combined value for all components $> 50 \text{ km s}^{-1}$ assuming the emission fills the beam, as described in the text by Andrew et al. (1978).

2004). Langer & Penzias (1990) find a ${}^{12}\text{C}/{}^{13}\text{C}$ ratio towards Sgr B2 of 24 ± 1 using observations of ${}^{12}\text{C}{}^{18}\text{O}$ and ${}^{13}\text{C}{}^{18}\text{O}$. However, the ${}^{13}\text{CH}$ lines are not detected in the ISO spectrum to a limit of 1.3% of the continuum (2σ level). This leads to ${}^{12}\text{CH}/{}^{13}\text{CH} > 36$ at the velocity of Sgr B2. This is higher than the value derived from CO but this could be due to isotopic fractionation which is expected to increase the ratio from the true ${}^{12}\text{C}/{}^{13}\text{C}$ value (see Langer et al. 1984). In the following analysis, we use the column density for Sgr B2 without adjustment.

The final CH column densities in Table 3 compare well with previous values derived from the KAO observations of same FIR lines by Stacey et al. (1987). Goicoechea et al. (2004) have also examined ISO data of CH and found absorption extended across the whole surrounding region. They calculate total column densities in the range $(0.8-1.8) \times 10^{15} \text{ cm}^{-2}$, peaking at the central Sgr B2 (M) and Sgr B2 (N) positions. Radio observations of the CH Λ -doublet lines by Andrew et al. (1978) are in very good agreement with the individual velocity features that we have fitted - the small discrepancies may be due to their much larger beam size ($8.2'$), which also included the (N) position. The radio lines were also observed by Genzel et al. (1979), however, they only give the column density for Sgr B2 itself at $+65 \text{ km s}^{-1}$ (although they also observed emission from the other velocity components). They derived the column density from the 3264 MHz line giving a value three times lower than ours (however, their weaker data for the 3335 MHz line would give a higher column density).

4.2. Ortho-CH₂

The lowest ortho level of CH₂ occurs at the ground level, $N=0$. We clearly detect absorption from the $1_{11}-0_{00}$ $J=2-1$ and $J=1-1$ fine structure components at 127 μm (see Fig. 2). The third component, $J=1-0$, is not detected above the noise in the spectrum. The observed features have a similar shape to the CH lines, indicating the presence of absorption along the whole line of sight.

The next highest energy level occurs ~ 67 K above ground. There are two transitions from this level that occur within the ISO wavelength range at 153 μm ($2_{11}-2_{02}$) and 94 μm ($3_{13}-2_{02}$), and one that occurs outside the range at 317 μm ($1_{11}-2_{02}$). The strongest fine-structure component of these is the $2_{11}-2_{02}$ $J=3-3$ line at 153.353 μm . However, this wavelength is very close to the $N=2-1$ $J=3-2$ transition of NH at 153.348 μm (separation ~ 10 km s $^{-1}$) and there is a strong absorption line detected (see Cernicharo et al. 2000). The identification of this feature with NH is secure because we also detect its $J=2-1$ and $J=1-0$ lines with relative depths that agree extremely well with the predicted line strengths (measured values are 1.0/0.55/0.27 compared to the predicted relative line strengths of 1.0/0.54/0.23 from the JPL line catalogue; Pickett et al. 1998). Furthermore, the next strongest CH₂ transition at 153.814 μm is not detected. This shows that the major contribution to the 153.35 μm line must be from NH rather than CH₂.

The next strongest transition is $3_{13}-2_{02}$ and the $J=4-3$ line (93.662 μm) should be almost as strong as the 153.35 μm line discussed above. There appear to be some features at roughly the correct velocity at a level $\sim 3\sigma$ above the statistical noise (see Fig. 2 but note that the error bars shown include systematic uncertainty).

No higher level ortho transitions were detected above the noise in the data.

4.3. Para-CH₂

The lowest energy state for para-CH₂ occurs at ~ 23 K above ground (see Fig. 1) and has two transitions at 156 μm ($1_{01}-1_{10}$) and 107 μm ($2_{12}-1_{10}$). The strongest fine-structure component of these is the $2_{12}-1_{10}$ $J=3-2$ transition at 107.720 μm . There is an absorption feature at approximately the correct wavelength for this line, although it appears to be wider than expected in its short wavelength wing. The observed absorption depth is also consistent with the data at the position of the next strongest component, $J=2-1$, at 107.857 μm (see Fig. 2). Using this detection to predict the optical depth of the strongest $1_{01}-1_{10}$ transition at 156.332 μm ($J=2-2$) gives a value consistent with the noise level in the spectrum.

No higher para transitions were detected above the noise in the data.

4.4. CH₂ column densities

In order to fit the CH₂ lines, we assumed that the relative column densities between each velocity feature were the same as for CH. This fixes the shape of the line and allows a single parameter fit to determine an 'average' CH/CH₂ column density

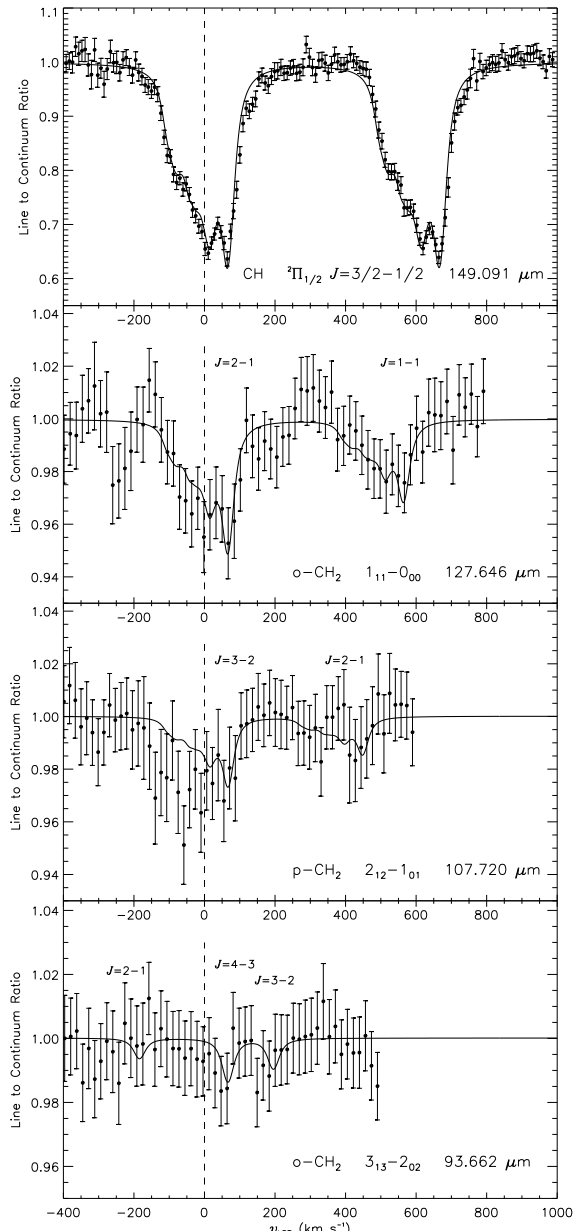


Fig. 2. **Upper panel:** Fit of the CH line towards Sgr B2 with the data binned at a quarter of the resolution element. **Lower panels:** In the lower three panels, a model based on the CH line shape has been fitted to the data around the three lowest energy transitions of CH₂. The relative contribution of each velocity component in these fits was fixed to the CH values in Table 3, except for the 94 μm ($3_{13}-2_{02}$) transition in the bottom plot which only includes the velocity component due to Sgr B2 itself (see text). The fit was carried out to the strongest fine structure component in each case. Other (sometimes undetected) components are included in the model using their expected relative line strengths from Table 1. The data are binned at half of the resolution element and the errors reflect both statistical noise and systematic error due to the dark current subtraction and continuum fit. The extra absorption feature seen at -250 km s $^{-1}$ relative to the 127 μm ($1_{11}-0_{00}$) transition appears to be real but is not identified.

ratio for each CH_2 energy level. The fit was carried out to the strongest fine structure component in each case, with the relative importance of the other (sometimes undetected) fine structure transitions fixed using the line strengths from Table 1. The results of these fits are shown in the lower 3 panels of Fig. 2 (including the undetected transitions, to show that their predicted absorption is consistent with non-detection in the data).

This method worked well for the strongest transition ($1_{11}-0_{00}$) at $127\text{ }\mu\text{m}$, where both the line shape and relative strength of the $J=2-1$ and $J=1-1$ components show a good fit. A detection limit for the $J=0-1$ component is also consistent with the expected line strengths of $1.0/0.6/0.2$ for $J=2-1$, $J=1-1$ and $J=0-1$ respectively. The fact that the line shape agrees well with the data indicates that the $[\text{CH}/\text{CH}_2]$ ratio does not vary significantly between the different line of sight components.

The para transition at $107.7\text{ }\mu\text{m}$ ($2_{12}-1_{01}$) does not show such good agreement in line shape with the model. As mentioned in Sect. 4.3, the main line appears wider than expected, although the noise is high in this part of the spectrum. It is unlikely that this extra absorption is associated with the CH_2 line as this would mean that the negative velocity features would have to be stronger than the component due to Sgr B2 itself and this is not observed in other lines. It could be due to overlap with an unidentified feature (although we have not been able to find a likely candidate) or an instrumental effect (e.g. the overlap of mini-scans can sometimes cause problems for wide lines - see Polehampton et al. 2003). A final possibility is that the extra absorption could have been introduced when dividing by the polynomial fit to the continuum. However, we minimised this effect by using a low order polynomial (3rd order) to carefully fit only the continuum around features that already appeared in the raw data. Any variation in the fitted baseline is on a larger scale than the excess absorption in the line. In fitting the line, we have only considered velocities above 0 km s^{-1} . The actual line shape is not well constrained by these data and our fitting method of fixing the relative contribution of each velocity to that of CH may overestimate the absorption due to the line of sight clouds.

In order to fit the data around the transition at $94\text{ }\mu\text{m}$ ($3_{13}-2_{02}$), we modified the line template to include only the velocity component at $+67\text{ km s}^{-1}$ from Table 3. This is because we only expect a significant population in the higher levels at the velocity of Sgr B2 itself. In Sgr B2 itself, excitation to the 2_{02} level ($\sim 67\text{ K}$ above ground) can be provided by FIR photons from the strong dust continuum, whereas in the line of sight clouds there is no strong radiation field and the densities are too low for collisional excitation to be important. The bottom panel in Fig. 2 shows the results of the fit.

The small discrepancy in velocity between fit and data can be explained by the fact that the main feature is only 3σ above the noise. The uncertainty in the exact line wavelength is also relatively high for this transition as it has never been measured in the lab either in Cologne or by Sears et al. (1984). The difference between the value quoted in Table 1 and that by Sears et al. (1984) is $\sim 3\text{ km s}^{-1}$.

The final column densities for the lowest ortho and para levels of CH_2 were determined directly from the fitted $[\text{CH}/\text{CH}_2]$ ratio for each level, assuming that the distribution over fine struc-

ture levels is determined by the line strengths given in Table 1. The final best fit values summed over all velocities are,

$$N(0_{00}) = (2.9 \pm 0.3) \times 10^{14} \text{ cm}^{-2}$$

$$N(1_{01}) = (3.4 \pm 0.9) \times 10^{14} \text{ cm}^{-2}$$

The column density in the 2_{02} level at the velocity of Sgr B2 is, $N(2_{02})_{\text{SgrB2}} = (1.2 \pm 0.5) \times 10^{14} \text{ cm}^{-2}$. Treating this as an upper limit allows us to make a comparison with the ortho ground state (using only the Sgr B2 component) and estimate the excitation temperature for Sgr B2, giving $T_{\text{rot}} < 40^{+14}_{-11}\text{ K}$. In order for absorption to be seen, this excitation temperature must be lower than the temperature of the dust producing the FIR background. In Sgr B2 the dust temperature has been found to be $\sim 30\text{ K}$ (Goicoechea & Cernicharo 2001), and so our estimated excitation temperature is consistent within its errors. At this temperature we do not expect any higher levels to be significantly populated and do not detect any of the other higher transitions that occur within the spectral survey range ($2_{20}-1_{11}$ at $50.5\text{ }\mu\text{m}$; $2_{21}-1_{10}$ at $50.8\text{ }\mu\text{m}$ and $3_{12}-3_{03}$ at $148.8.5\text{ }\mu\text{m}$).

Assuming that only the first three energy levels in Sgr B2 are populated, the ortho-to-para ratio in the $+67\text{ km s}^{-1}$ component is $1.6^{+0.9}_{-0.6}$. The equilibrium value of the ratio for CH_2 should be ≥ 3 for low temperatures. This difference could be a relic of the formation process with the current ortho-to-para ratio fixed at formation and/or set by the ratio of the parent species. Alternatively, it could indicate that not all of the $2_{12}-1_{01}$ absorption seen at $107.7\text{ }\mu\text{m}$ is associated with CH_2 , possibly due to blending with another line. Reducing the para column density by approximately a factor of 2 would lead to an ortho-to-para ratio of 3.

Overall, the column density summed over all velocities in both ortho and para states is $N(\text{CH}_2) = (7.5 \pm 1.1) \times 10^{14} \text{ cm}^{-2}$, giving a final ratio with CH of $[\text{CH}/\text{CH}_2] = 2.7 \pm 0.5$. If the para column density is reduced to make the ortho-to-para ratio equal to 3, the $[\text{CH}/\text{CH}_2]$ ratio would be increased to 3.7.

5. Abundances

To discuss CH and CH_2 abundances, we need an estimate of the hydrogen column density towards Sgr B2.

In the Galactic spiral arm clouds along the line of sight (-100 to $+30\text{ km s}^{-1}$), HCN and CS measurements suggest average densities of 200 cm^{-3} , but also the presence of gas up to 10^4 cm^{-3} (Greaves 1995). Their structure is probably similar to photodissociation regions (PDRs) with a molecular core and atomic skin at the surface, and UV illumination provided by the mean interstellar radiation field (Vastel et al. 2002). $N(\text{H}_2)$ has been estimated to be 5, 9, 4 and $14 \times 10^{21} \text{ cm}^{-2}$ respectively in the -100 , -40 , -25 and 0 km s^{-1} features (Greaves & Nyman 1996), with corresponding atomic hydrogen column densities approximately equal to 2, 4, 2 and $8 \times 10^{21} \text{ cm}^{-2}$ (Vastel et al. 2002). In order to compare with diffuse cloud models, we calculate the abundances taking into account the total hydrogen particle column, $N_{\text{H}} = N(\text{H}) + 2N(\text{H}_2)$, although it is difficult to determine whether the observed CH and CH_2 co-exists with both atomic and molecular hydrogen regions - they are probably confined to one or more specific layers within each cloud.

Using our fitted column densities for CH in Table 3, we calculate an approximate abundance of $N(\text{CH})/N_{\text{H}} \sim (0.6\text{--}3) \times 10^{-8}$ for these clouds. According to our average $[\text{CH}/\text{CH}_2]$ ratio, $N(\text{CH}_2)/N_{\text{H}}$ is thus $(0.2\text{--}1.1) \times 10^{-8}$.

The situation is more complicated at the velocity of Sgr B2 as there may be contributions to the absorption from layers with widely different conditions. Comito et al. (2003) have found that a significant fraction of the water absorption towards Sgr B2 must be due to a hot (500–700 K), low density layer (also observed in ammonia lines; Ceccarelli et al. 2002; Hüttemeister et al. 1995) but that there must also be absorption from the warm (40–80 K) envelope. Goicoechea & Cernicharo (2002) have derived a large OH abundance at the velocity of Sgr B2 suggesting that there is a strong UV field producing clumpy PDRs and a temperature gradient from 40–600 K through the envelope. The total H_2 column density in front of the FIR continuum has been estimated from the FIR spectrum to be $(2\text{--}10) \times 10^{23} \text{ cm}^{-2}$ (Goicoechea & Cernicharo 2001). Using this to calculate approximate abundances gives $N(\text{CH})/N_{\text{H}} \sim (0.5\text{--}2) \times 10^{-9}$ and $N(\text{CH}_2)/N_{\text{H}} \sim (0.2\text{--}0.7) \times 10^{-9}$.

6. CH_2 in other sources

We have also searched the ISO Data Archive for observations towards other sources that may show the low-lying CH_2 lines.

6.1. W49 N

Observations that cover the wavelengths of the CH_2 lines were carried out using the LWS L04 mode towards the active star forming region, W49 N. This is the strongest IR peak in the W49 A molecular cloud complex which is located at 11.4 kpc from the Sun and 8.1 kpc from the Galactic Centre (Gwinn et al. 1992). Its spectrum shows a strong thermal continuum in the FIR with a peak near $60 \mu\text{m}$ (Vastel et al. 2001). Line emission associated with the molecular cloud itself is centred at 8 km s^{-1} (e.g. Jaffe et al. 1987), but there are also several features due to intervening gas at velocities between 16 and 75 km s^{-1} (e.g. Nyman 1983). Vastel et al. (2000) have mapped the CO emission in the ISO LWS beam and found 7 velocity components in the range $35\text{--}70 \text{ km s}^{-1}$. Recently, Plume et al. (2004) have measured H_2O towards W49 and the same features show up in absorption. They arise because the line of sight intersects the Sagittarius spiral arm in two places (e.g. Greaves & Williams 1994).

The strongest ortho- CH_2 $1_{11}-0_{00}$ fine structure component at $127.6 \mu\text{m}$ ($J=2-1$) is clearly detected in absorption in the LWS FP spectrum. However, the spectral resolution and signal-to-noise ratio in the data do not allow a detailed fit using all the velocity components observed in CO and H_2O lines. Therefore, we performed a simplified fit using two components to represent the strongest features seen in the H_2O spectrum of Plume et al. (2004). We fixed the velocities (and FWHM) to be 37 km s^{-1} (10 km s^{-1}) and 61 km s^{-1} (7 km s^{-1}) and found the best fitting optical depths after convolving to the LWS resolution. Lower velocity components were not necessary to reproduce the line shape, showing that all the absorption comes from the line of sight clouds. Only the $J=2-1$ component was used

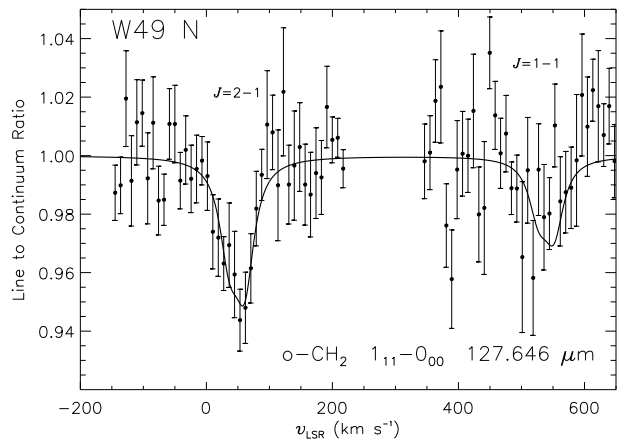


Fig. 3. Data around the $J=2-1$ ($127.6 \mu\text{m}$) and $J=1-1$ ($127.8 \mu\text{m}$) fine structure components of the $1_{11}-0_{00}$ CH_2 transition toward W49 N. The solid line shows a model derived from a fit to the $J=2-1$ component and the expected relative line strength of the $J=1-1$ component.

for the fit. The result is shown in Fig. 3, which also shows a prediction for the $J=1-1$ ($127.858 \mu\text{m}$) fine structure component based on its expected relative line strength. Column densities for the 0_{00} level, calculated from the best fitting optical depths and equation 2, are $(0.8 \pm 0.4) \times 10^{14} \text{ cm}^{-2}$ and $(1.2 \pm 0.4) \times 10^{14} \text{ cm}^{-2}$ at 37 km s^{-1} and 61 km s^{-1} respectively.

The para transition at $107 \mu\text{m}$ ($2_{12}-1_{01}$) is not detected above the noise. Assuming that only the two lowest levels are populated and using a 2σ limit on the line depth, gives an ortho-to-para ratio > 2.1 .

The CH line at $149 \mu\text{m}$ was not observed toward W49 N using the FP mode of the LWS, but it was measured with the lower resolution grating mode. At this resolution the Λ -doublet line splitting, as well as the line of sight structure, is not resolved and we can only estimate a total CH column density that may include absorption associated with W49 itself, giving $8.4 \times 10^{14} \text{ cm}^{-2}$. Sume & Irvine (1977) have observed CH radio Λ -doublet lines towards W49 A and they find column densities of $8 \times 10^{13} \text{ cm}^{-2}$ and $10 \times 10^{13} \text{ cm}^{-2}$ in the velocity intervals $30\text{--}45 \text{ km s}^{-1}$ and $54\text{--}72 \text{ km s}^{-1}$. Rydbeck et al. (1976) also observed the Λ -doublet lines, giving column densities of $7 \times 10^{13} \text{ cm}^{-2}$ and $18 \times 10^{13} \text{ cm}^{-2}$. Both authors show that these two velocity intervals give the most important CH contributions. This means the extra column density seen in the LWS grating measurement probably also has highest contribution from these ranges and the radio measurements may be an underestimate (probably due to the much larger beam size of $15'$ used for these observations).

Using the average of the two radio CH measurements and combining the ortho column density and para upper limit for CH_2 , gives a lower limit for the $[\text{CH}/\text{CH}_2]$ ratio of 1.4 and 0.8 in the two velocity intervals.

6.2. Sgr A*

Observations using the LWS FP mode were also made towards Sgr A* at the Galactic Centre. It has a FIR continuum show-

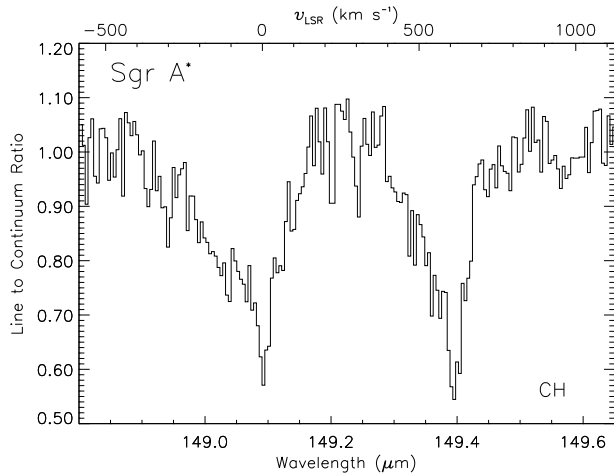


Fig. 4. The CH $^2\Pi_{1/2}$ $J=3/2-1/2$ transition observed towards Sgr A* showing two resolved Λ -doublet components.

ing strong thermal emission from dust, peaking at ~ 50 μm . Observations of several hydrocarbons have been reported towards this source, including CH₃ (Feuchtgruber et al. 2000). We have searched LWS FP observations for the lines of CH₂ and CH and Fig. 4 shows the observed absorption due to the $^2\Pi_{1/2}$ $J=3/2-1/2$ (149 μm) rotational transition of CH. These lines show peak absorption near 0 km s^{-1} , probably due to local gas. There is also absorption at negative velocities due to galactic spiral arm clouds. This picture is consistent with observations of CH Λ -doublet lines towards Sgr A, which showed that the strong Galactic Centre component normally observed in other molecules at $+50$ km s^{-1} is relatively weak in CH (Genzel et al. 1979). At the wavelength of the ortho CH₂ $1_{11}-0_{00}$ transition (127 μm), the signal-to-noise ratio in the data is rather low compared to the Sgr B2 observations and we do not detect any absorption. The para $2_{12}-1_{01}$ transition at 107.7 μm is also not detected. Combining 2σ upper limits for both transitions, we calculate a lower limit to the [CH/CH₂] ratio at 0 km s^{-1} of 2.6.

6.3. NGC7023

The ISO database also contains LWS FP observations of CH₂ towards three positions in the NGC7023 PDR. However, no lines are detected above the noise in the spectra. This is consistent with LWS grating observations in which no OH, CH or CH₂ were detected toward any position in NGC7023 (Fuente et al. 2000).

7. Discussion

7.1. Comparison with models

In Table 4 we summarise the results from several chemical models for diffuse (van Dishoeck & Black 1986) and dense clouds (Lee et al. 1996), as well as a recent model that takes both gas-phase and grain-surface chemistry into account (Ruffle & Herbst 2001). In these models, the abundances of CH and CH₂ are generally predicted to be higher towards lower densities and temperatures. We also include the results from a

PDR model of the IC63 nebula from Jansen et al. (1995) - this is thought to have similar physical conditions to the Sgr B2 envelope ($n \sim 10^5 \text{ cm}^{-3}$; 650–900 times the average interstellar UV field). In this model, CH and CH₂ peak towards the edge of the PDR at $A_V < 2$, with [CH/CH₂] generally ~ 2 (although in a model with higher fractional abundance of carbon they calculated a value ~ 20). The CH abundance reached is relatively high compared to the dense cloud models with similar n_{H} . In PDR models with higher density and more intense UV fields, even larger CH and CH₂ abundances can be reached in the outer layers (Sternberg & Dalgarno 1995).

Table 4 compares our estimated abundances with the models. In the line of sight clouds towards Sgr B2 (-100 to $+30 \text{ km s}^{-1}$), Greaves & Nyman (1996) have examined the abundances of 11 species observed at 3 mm (HCO⁺, HCN, HNC, CN, CCH, C₃H₂, CS, SiO, N₂H⁺, CH₃OH and SO) and found that overall, the chemistry in these features is similar to the dark cloud TMC1. However, our abundances are much closer to diffuse cloud values, showing that CH and CH₂ may reside in the less dense parts of the clouds. In Sgr B2 itself, our derived abundances are much more uncertain due to the difficulty in estimating $N(\text{H})$, but are lower than the line of sight clouds, consistent with denser material in Sgr B2.

We can also compare our results with the previous observations of CH₂ in diffuse (Lyu et al. 2001) and dense clouds (Hollis et al. 1995). Using the results of Lyu et al. (2001) with hydrogen abundances for their lines of sight (see van Dishoeck & Black 1986; Snow et al. 1996), we calculate value consistent with our line of sight values and the diffuse cloud model listed in Table 4. For the high densities and temperatures prevailing in the Orion-KL and W51 M hot cores, Hollis et al. (1995) derive $X(\text{CH}_2) \approx 4 \times 10^{-9}$ and 7×10^{-10} , respectively, carefully considering beam-filling factors. These values are closer to our results for Sgr B2.

7.2. CH/CH₂ chemistry

Both CH and CH₂ are formed by the dissociative recombination of CH₃⁺ and primarily destroyed by reaction with atomic oxygen to form HCO, a constituent of many more complex molecules. Hollis et al. (1995) compared their derived CH₂ abundance in the Orion-KL and W51 M hot cores with radio observations of CH to determine branching ratios for the formation of CH and CH₂ of 0.1 and 0.9 respectively. The actual branching ratios for the dissociative recombination of CH₃⁺ have since been measured in the lab by Vejby-Christensen et al. (1997). There are 4 important pathways, with CH₂ as the major product (40%), two reactions producing CH (30%) and the remainder producing atomic carbon (30%). This appears to agree with models of diffuse and translucent clouds, which required a high abundance of CH₂ to reproduce the measured column densities of C₂ (van Dishoeck & Black 1986, 1989).

The above discussion indicates that CH₂ should be more abundant than CH. However, our observations show that in the line of sight towards Sgr B2, CH₂ has less than half the abundance of CH - if this were not the case, we would have detected much stronger CH₂ absorption. The observations to-

Table 4. Comparison of model predictions for diffuse and dense clouds with the observed abundances (compared to $2N(\text{H}_2) + N(\text{H})$) of CH and CH_2 ($X(\text{CH})$ and $X(\text{CH}_2)$). The diffuse cloud model is for the line of sight to ζ Per (van Dishoeck & Black 1986): vDB86. The quoted density and temperature are for the centre of the cloud in the model. The dense cloud models are steady state values corresponding to the gas phase “new standard model” of Lee et al. (1996): L96 and the gas-grain model of Ruffle & Herbst (2001): RH01 including photochemistry (P1/A at 10^8 yr). The PDR model is for a density of 10^5 cm^{-3} and radiation field ~ 650 – 900 times the average interstellar value (Jansen et al. 1995): J95. The observational results derived from our ISO measurements are shown as well as previous results from Lyu et al. (2001) and Hollis et al. (1995).

		Density (cm^{-3})	Temperature (K)	$X(\text{CH})$ (10^{-8})	$X(\text{CH}_2)$ (10^{-8})	$[\text{CH}/\text{CH}_2]$
Model predictions:	Diffuse (vDB86)	500	25	1.6	2.4	0.67
	Dense (L96)	10^3	10	0.25	1.6	0.018
	Dense (L96)	10^5	10	0.0007	0.039	0.16
	Dense (RH01)	2×10^4	10	0.1	1.2	0.08
	PDR (J95)	10^5		1.4	0.7	2.0
Results from this work:	Sgr B2 Line of Sight			0.6–3	0.2–1.1	2.7 ± 0.5
	Sgr B2			0.05–0.2	0.02–0.07	2.7 ± 0.5
	W49 N 37 km s ⁻¹					>1.4
	W49 N 61 km s ⁻¹					>0.8
	Sgr A*					>2.6
Previous observational results:	ζ Oph			1.8 ^b	4.3 ^a	0.4 ^b
	HD154368			1.9 ^d	0.79 ^c	2.4 ^d
	Orion-KL	$\sim 10^5$	100–200	0.06 ^e	0.4 ^e	0.1 ^e
	W51 M	$\sim 10^4$	100–200	0.007 ^e	0.07 ^e	0.1 ^e

^a Combining $N(\text{CH}_2)$ from Lyu et al. (2001) with a hydrogen column density as quoted in van Dishoeck & Black (1986).

^b Based on $N(\text{CH})=2.5 \times 10^{13} \text{ cm}^{-2}$ from van Dishoeck & Black (1989).

^c Combining $N(\text{CH}_2)$ from Lyu et al. (2001) with a hydrogen column density from Snow et al. (1996).

^d Based on $N(\text{CH})=8 \times 10^{13} \text{ cm}^{-2}$ from van Dishoeck & Black (1989).

^e Taking values as quoted by Hollis et al. (1995) - but note that $X(\text{CH})$ could be significantly higher - see text.

wards W49 and the non-detection towards Sgr A* also appear to confirm this. Furthermore, the results of Lyu et al. (2001) towards HD154368 combined with previous measurements of CH (see Table 4) show very good agreement with the Sgr B2 ratio.

These results are contrary to the previous observations towards Orion-KL and W51 M where CH_2 was found to be 10 times more abundant than CH. This may be due to the difficulty in determining the CH column density equivalent to the measured CH_2 emission in these sources. Hollis et al. (1995) used CH column densities derived by Rydbeck et al. (1976), giving $N(\text{CH}) = 2 \times 10^{13} \text{ cm}^{-2}$ towards W51 M. In contrast, Turner (1988) made a detailed study of the Λ -doublet satellite lines from the first rotationally excited state towards W51, giving a value for the 57 km s⁻¹ velocity component that is more than 100 times larger: $6.2 \times 10^{15} \text{ cm}^{-2}$. This indicates that $[\text{CH}/\text{CH}_2]$ could be as high as 30, although the radio CH line observations are likely to sample a much larger and cooler region than the 70 GHz CH_2 lines which require high temperatures to be excited.

This shows it is extremely important to have consistent measurements of CH and CH_2 (with transitions at similar energies, using the same beam size and with consistent calibration) in order to be able to make a good comparison. So far the current data towards Sgr B2 provides the best comparison of the two species.

In order to explain the low abundance of CH_2 with respect to CH observed towards Sgr B2, we require other formation/destruction processes to be important for the CH/CH_2 balance. The PDR model of Jansen et al. (1995) shows that the presence of strong UV radiation can reproduce our observed $[\text{CH}/\text{CH}_2]$ ratio. This may explain the ratio in Sgr B2 but in the galactic spiral arm clouds, the UV field is much weaker and densities lower than used by Jansen et al. (1995). Viti et al. (2000) have modelled the hydrocarbon chemistry in diffuse and translucent clouds ($n=300 \text{ cm}^{-3}$) including the interaction of gaseous C⁺ with dust grains. This leads to the production of hydrocarbons by surface reactions. In some of their models (for $A_v=4$), they find column densities approaching those that we find in the line of sight clouds towards Sgr B2 and $[\text{CH}/\text{CH}_2]$ ratios 7.7–13.6. These surface reactions could explain our high observed $[\text{CH}/\text{CH}_2]$ ratio.

8. Summary

We have made the first detection of the low-lying rotational transitions of the CH_2 molecule in the ISM towards Sgr B2 and W49 N in absorption. We do not detect CH_2 towards Sgr A* or NGC7023. For Sgr B2 we were able to compare these observations with measurements of the ground state rotational lines of CH, providing a good estimate of the total column density of both species along the line of sight. These observations provide the best comparison of the two species to date, giving a

[CH/CH₂] ratio of 2.7±0.5, probably fairly constant in all the observed velocity components. The results towards W49 N appear to agree with this ratio, giving a lower limit of ∼1.0.

Comparison with chemical models shows that the abundances in the line of sight clouds are close to diffuse cloud conditions whereas in Sgr B2 itself they indicate denser gas is present. Our high [CH/CH₂] ratio can be explained by models including grain surface reactions (e.g. Viti et al. 2000).

Future observations in the FIR with SOFIA and in the sub-millimetre with telescopes such as the Atacama Pathfinder Experiment (APEX) will be highly interesting to extend the study of CH₂ to other sources.

Acknowledgements. We wish to thank T. W. Grundy (RAL) for supplying us with the LWS grating spectrum of W49 N processed using the latest version of the strong source correction and L01 post-processing pipeline. The LWS Interactive Analysis (LIA) package is a joint development of the ISO-LWS Instrument Team at the Rutherford Appleton Laboratory (RAL, UK - the PI Institute) and the Infrared Processing and Analysis Center (IPAC/Caltech, USA). The ISO Spectral Analysis Package (ISAP) is a joint development by the LWS and SWS Instrument Teams and Data Centres. Contributing institutes are CESR, IAS, IPAC, MPE, RAL and SRON.

References

Andrew, B. H., Avery, L. W., & Brotan, N. W. 1978, A&A, 66, 437

Brünken, S., Michael, E. A., Lewen, F., et al. 2004, Can. J. Chem., 82, 676

Bunker, P. R. & Langhoff, S. R. 1983, J. Molec. Spectrosc., 102, 204

Ceccarelli, C., Baluteau, J.-P., Walmsley, M., et al. 2002, A&A, 383, 603

Cernicharo, J., Goicoechea, J. R., & Caux, E. 2000, ApJ, 534, L199

Cernicharo, J., Orlandi, M. A., González-Alfonso, E., & Leeks, S. J. 1999, in The Universe as seen by ISO, ESA SP-427, 655

Chandra, S. 1984, Ap&SS, 98, 269

Clegg, P. E., Ade, P. A. R., Armand, C., et al. 1996, A&A, 315, L38

Comito, C., Schilke, P., Gerin, M., et al. 2003, A&A, 402, 635

Davidson, S. A., Evenson, K. M., & Brown, J. M. 2001, ApJ, 546, 330

Davidson, S. A., Evenson, K. M., & Brown, J. M. 2004, J. Mol. Spectrosc., 223, 20

Douglas, A. E. 1951, ApJ, 114, 466

Feuchtgruber, H., Helmich, F. P., van Dishoeck, E. F., & Wright, C. M. 2000, ApJ, 535, L111

Fuente, A., Martín-Pintado, J., Roderíguez-Fernández, N. J., Cernicharo, J., & Gerin, M. 2000, A&A, 354, 1053

Garwood, R. W. & Dickey, J. M. 1989, ApJ, 338, 841

Genzel, R., Downes, D., Pauls, T., Wilson, T. L., & Bieging, J. 1979, A&A, 73, 253

Goicoechea, J. R. & Cernicharo, J. 2001, ApJ, 554, L213

Goicoechea, J. R. & Cernicharo, J. 2002, ApJ, 576, L77

Goicoechea, J. R., Roderíguez-Fernández, N. J., & Cernicharo, J. 2004, ApJ, 600, 214

Greaves, J. S. 1995, MNRAS, 273, 918

Greaves, J. S. & Nyman, L. 1996, A&A, 305, 950

Greaves, J. S. & Williams, P. G. 1994, A&A, 290, 259

Gry, C., Swinyard, B., Harwood, A., et al. 2003, ISO Handbook Volume III (LWS), Version 2.1, ESA SAI-99-077/Dc

Gwinn, C. R., Moran, J. M., & Reid, M. J. 1992, ApJ, 393, 149

Herzberg, G. 1942a, Reviews of Modern Physics, 14, 195

Herzberg, G. 1942b, ApJ, 96, 314

Hollis, J. M., Jewell, P. R., & Lovas, F. J. 1989, ApJ, 346, 794

Hollis, J. M., Jewell, P. R., & Lovas, F. J. 1995, ApJ, 438, 259

Hüttemeister, S., Wilson, T. L., Mauersberger, R., et al. 1995, A&A, 294, 667

Jaffe, D. T., Harris, A. I., & Genzel, R. 1987, ApJ, 316, 231

Jansen, D. J., van Dishoeck, E. F., Black, J. H., Spaans, M., & Sosin, C. 1995, A&A, 302, 223

Langer, W. D., Graedel, T. E., Frerking, M. A., & Armentrout, P. B. 1984, ApJ, 277, 581

Langer, W. D. & Penzias, A. A. 1990, ApJ, 357, 477

Lee, H.-H., Bettens, R. P. A., & Herbst, E. 1996, A&AS, 119, 111

Lim, T. L., Hutchinson, G., Sidher, S. D., et al. 2002, SPIE, 4847, 435

Lloyd, C., Lerate, M. R., & Grundy, T. W. 2003, The LWS L01 Pipeline, version 1, available from the ISO Data Archive at <http://www.iso.vilspa.esa.es/ida/>

Lovas, F. J., Suenram, R. D., & Evenson, K. M. 1983, ApJ, 267, L131

Lyu, C.-H., Smith, A. M., & Bruhweiler, F. C. 2001, ApJ, 560, 865

Michael, E. A., Lewen, F., Winnewisser, G., et al. 2003, ApJ, 596, 1356

Nyman, L.-Å. 1983, A&A, 120, 307

Pickett, H. M., Poynter, R. L., Cohen, E. A., et al. 1998, J. Quant. Spectrosc. & Rad. Transfer, 60, 883

Plume, R., Kaufman, M. J., Neufeld, D. A., et al. 2004, ApJ, 605, 247

Polehampton, E. T., Baluteau, J.-P., Ceccarelli, C., Swinyard, B. M., & Caux, E. 2002, A&A, 388, L44

Polehampton, E. T., Brown, J. M., Swinyard, B. M., & Baluteau, J.-P. 2003, A&A, 406, L47

Ruffle, D. P. & Herbst, E. 2001, MNRAS, 322, 770

Rydbeck, O. E. A., Kollberg, E., Hjalmarson, Å., et al. 1976, ApJS, 31, 333

Sears, T. J., McKellar, A. R. W., Bunker, P. R., Evenson, K. M., & Brown, J. M. 1984, ApJ, 276, 399

Snow, T. P., Black, J. H., van Dishoeck, E. F., et al. 1996, ApJ, 465, 245

Spitzer, L. 1978, Physics of the Interstellar Medium (New York: John Wiley and Sons)

Stacey, G. J., Lugten, J. B., & Genzel, R. 1987, ApJ, 313, 859

Sternberg, A. & Dalgarno, A. 1995, ApJS, 99, 565

Sturm, E., Bauer, O. H., Lutz, D., et al. 1998, in Astronomical Data Analysis Software and Systems VII, ASP Conference Series 145, 161

Sume, A. & Irvine, W. M. 1977, A&A, 60, 337

Swinyard, B. M., Burgdorf, M. J., Clegg, P. E., et al. 1998, SPIE, 3354, 888

Turner, B. E. 1988, ApJ, 329, 425

van Dishoeck, E. F. & Black, J. H. 1986, *ApJS*, 62, 109
 van Dishoeck, E. F. & Black, J. H. 1989, *ApJ*, 340, 273
 Vastel, C., Caux, E., Ceccarelli, C., et al. 2000, *A&A*, 357, 994
 Vastel, C., Polehampton, E. T., Baluteau, J.-P., et al. 2002, *ApJ*, 581, 315
 Vastel, C., Spaans, M., Ceccarelli, C., Tielens, A. G. G. M., & Caux, E. 2001, *A&A*, 376
 Vejby-Christensen, L., Andersen, L. H., Heber, O., et al. 1997, *ApJ*, 483, 531
 Viti, S., Williams, D. A., & O'Neill, P. T. 2000, *A&A*, 354, 1062

Appendix A: Observations used

Table A.1. Log of the observations used.

Transition	Observing Mode	ISO TDT Number	LWS Detector	Resolution (km s ⁻¹)
¹²CH and ¹³CH Sgr B2				
<i>J</i> =3/2–1/2 (149 μm) (& para-CH ₂ 3 ₁₂ –3 ₀₃ ^a)	L03	50700208	LW3	36
	L03	84500102	LW3	36
	L03	50600603	LW3	36
	L03	50600814	LW4	36
	L03	50900521	LW4	36
<i>J</i> =3/2–5/2 (115 μm) ^a	L03	50601013	LW2	34
ortho-CH₂ Sgr B2				
1 ₁₁ –0 ₀₀ (127 μm)	L03	50700511	LW2	34
	L03	50800819	LW3	34
	L04	47600907	LW2	34
2 ₁₁ –2 ₀₂ (153 μm) ^a	L03	50700208	LW4	35
	L03	50800317	LW4	35
	L03	50400823	LW4	35
	L03	50600405	LW3	35
	L03	83600317	LW3	35
3 ₁₃ –2 ₀₂ (94 μm)	L03	50800218	LW1	34
	L03	50400823	LW1	34
	L03	50700610	LW1	34
2 ₂₀ –1 ₁₁ (50 μm) ^a	L03	50800218	SW2	64
para-CH₂ Sgr B2				
1 ₁₀ –1 ₀₁ (156 μm) ^b	L03	50700707	LW4	35
	L03	50700610	LW4	35
	L03	50800317	LW4	35
2 ₁₂ –1 ₀₁ (107 μm)	L03	50800515	LW2	32
	L03	50800819	LW2	32
2 ₂₁ –1 ₁₀ (51 μm) ^a	L03	50800216	SW2	64
	L03	50600814	SW2	64
	L03	50700511	SW2	64
	L03	50900521	SW2	64
CH₂ W49 N				
1 ₁₁ –0 ₀₀ (127 μm)	L04	49900406	LW2	34
2 ₁₂ –1 ₀₁ (107 μm) ^a	L04	49900406	LW2	32
CH W49 N				
<i>J</i> =3/2–1/2 (149 μm)	L01	52700702	LW4	1200
CH₂ Sgr A*				
1 ₁₁ –0 ₀₀ (127 μm) ^a	L03	50900204	LW2	34
2 ₁₂ –1 ₀₁ (107 μm) ^a	L03	50800902	LW2	32
	L03	85000139	LW2	32
	L03	50900444	LW1	32
	L03	85000247	LW1	32
CH Sgr A*				
<i>J</i> =3/2–1/2 (149 μm)	L03	84900448	LW3	34
CH₂ NGC7023 (3 different positions)				
1 ₁₁ –0 ₀₀ (127 μm) ^a	L04	33901603	LW2	34
	L04	34601501	LW2	34
	L04	56000208	LW2	34

^a Not detected.

^b Blended with NH line.